



Tunable broadband terahertz polarizer using graphene-metal hybrid metasurface

K. MENG,¹ S. J. PARK,¹ L. H. LI,¹ D. R. BACON,¹ L. CHEN,¹ K. CHAE,³ J. Y. PARK,³ A. D. BURNETT,² E. H. LINFIELD,¹ A. G. DAVIES,¹ AND J. E. CUNNINGHAM^{1,*}

¹School of Electronic and Electrical Engineering, University of Leeds, Woodhouse Lane, Leeds, LS2 9JT, United Kingdom

²School of Chemistry, University of Leeds, Woodhouse Lane, Leeds, LS2 9JT, United Kingdom

³Department of Physics and Department of Energy Systems Research, Ajou University, Suwon 16499, South Korea

*j.e.cunningham@leeds.ac.uk

Abstract: We demonstrate an electrically tunable polarizer for terahertz (THz) frequency electromagnetic waves formed from a hybrid graphene-metal metasurface. Broadband (>3 THz) polarization-dependent modulation of THz transmission is demonstrated as a function of the graphene conductivity for various wire grid geometries, each tuned by gating using an overlaid ion gel. We show a strong enhancement of modulation (up to ~ 17 times) compared to graphene wire grids in the frequency range of 0.2–2.5 THz upon introduction of the metallic elements. Theoretical calculations, considering both plasmonic coupling and Drude absorption, are in good agreement with our experimental findings.

Published by The Optical Society under the terms of the [Creative Commons Attribution 4.0 License](#). Further distribution of this work must maintain attribution to the author(s) and the published article's title, journal citation, and DOI.

1. Introduction

Components to enhance and extend the capability of THz spectroscopies have been intensively developed in the past few decades, including efficient antennas [1], switches [2], absorbers [3], and biosensors [4–6]. THz polarizers are essential for removing unwanted polarization components and / or of controlling the polarization state of THz waves and hence are important components in many THz systems and applications [7,8]. Several polarizers for THz radiation have previously been reported, including those formed from liquid crystals [9], semiconductors [10], metal wire grids [11], carbon nanotubes [12], and graphene [13]. Particular emphasis has been placed on graphene, owing to its electrically tunable optical (including THz) conductivity [14], which allows for tunable (Drude) absorption [15]. Graphene is also ideal for such applications since its plasmon resonance, which can be fine-tuned by changing its geometry [16–18], lies in the mid-infrared to THz frequency range [19].

Several different schemes for THz polarizers incorporating graphene have been presented previously [20]. Metasurfaces are comprised of two-dimensional arrays of elements capable of anisotropic manipulation of EM waves [21]. They offer a promising approach to achieving tunable THz polarizers, either in the form of pure graphene metasurfaces [13,22,23], or through the incorporation of sheets of graphene into metal metasurfaces [8,24]. These structures have shown their capability to control the polarization direction [8,23,24] and to manipulate polarization by converting between linear and circular polarization states, for example [13,22,23]. Compared with reports on the manipulation of the polarization state, THz amplitude modulation, and especially broadband modulation, is less common, despite the importance of being able to tune the amplitude of a desired polarization for the development of spatial light modulators [25] for

THz communications [26] for example. More importantly, studying tunable THz polarizers is essential for developing THz switching and attenuator devices for THz communications [27].

THz polarizers formed from wire grids (either free-standing [28] or on a substrate [29]) have a low insertion loss (1 dB) and high polarization extinction ratio (PER) (up to ~40 dB in the range 0.3–1 THz) [11]. Such metallic wire-grid polarizers typically show a low transmission for transverse electric (TE) polarized waves and a high transmission for transverse magnetic (TM) polarized waves [28]. The same is true for wire grids formed from graphene, both in the near-infrared [30,31], and in the microwave regions of the electromagnetic spectrum [32], while at THz frequencies, they typically show a low transmission for TM-polarized THz waves owing to THz wave-plasmon coupling [17,33]; this thus represents a limitation of pure graphene wire grid based polarizers. A further limitation is the low modulation (~10%) of the TE transmission, which is caused by Drude absorption [17].

In this paper, we report on the design, fabrication and characterization of broadband tunable THz polarizers utilizing graphene-metal hybrid wire grids. Compared with previous hybrid graphene-metal metasurface polarizers that employ sheets of graphene covering the whole metal metasurface area [8,24], our design is that of a hybrid graphene-wire grid and metal metasurface which allows both the graphene and the metal elements of the design to contribute to the anisotropic properties of the polarizer, providing a significant PER enhancement. Our design also overcomes two drawbacks of graphene wire grid THz polarizers, namely their weak modulation and the THz wave-plasmon coupling, which restrict the TM transmission [17]. Our polarizer shows a broadband (up to several THz) polarization-dependent modulation, with an up to ~17 times enhancement of modulation ability in the range 0.5–2.5 THz compared with a graphene-wire grid polarizer containing no metal.

2. Design and methods

2.1. Design and principle

Our graphene-metal hybrid wire grid structure, comprising a graphene wire grid overlaid on to a metal metasurface such that the graphene and metal elements are interleaved, is shown in Fig. 1(a). The metal metasurface is formed from a metal patch array. The introduction of metal makes the sheet conductivity of the graphene-metal hybrid wires larger than wires formed from graphene alone. The conductivity of the hybrid wires is given by

$$\sigma_s = (L_{\text{graphene}}/(\sigma_{\text{graphene}} \times \Lambda_{G/M}) + L_{\text{metal}}/(\sigma_{\text{metal}} \times \Lambda_{G/M}))^{-1} \quad (1)$$

where, σ_{graphene} and σ_{metal} are the sheet conductivity of graphene and metal, respectively, and L_{graphene} , L_{metal} , and $\Lambda_{G/M}$ are the dimension of graphene, metal patch and period of graphene-metal structure along the wires, respectively, as shown in Fig. 1(a). Since the sheet conductivity of the metal is much larger than that of graphene, we can write $\Delta\sigma_s \approx \Delta\sigma_{\text{graphene}} \times \Lambda_{G/M}/L_{\text{graphene}}$ to a reasonable approximation. Thus, smaller graphene filling factors (GFF) along the wire, $L_{\text{graphene}}/\Lambda_{G/M}$, lead to a larger conductivity modulation, which in turn results in a larger THz transmission modulation. The strong TM-polarized plasmon mode present in graphene wires is suppressed by the introduction of the metal metasurface, which effectively acts to transform the graphene wires into separated graphene patches connected by metal. The EM wave-to-plasmon coupling efficiency of the graphene patches is determined by their dimensions, and for a certain width, the TM-polarized coupling is highly suppressed by decreasing L_{graphene} [34]. As well as this suppression, the metal metasurface introduces a TE-polarized plasmon into graphene, whose interaction with THz wave is then tunable by modulating the conductivity of graphene; this TE-polarized plasmon also contributes to the THz transmission modulation [35]. The generated TE-polarized plasmon is induced by the THz wave coupling to the resonance of an inductive-capacitive (LC) circuit formed by the metal-graphene structure, in which the metal acts as a capacitive reservoir for charge accumulation and the graphene serves as an inductive channel.

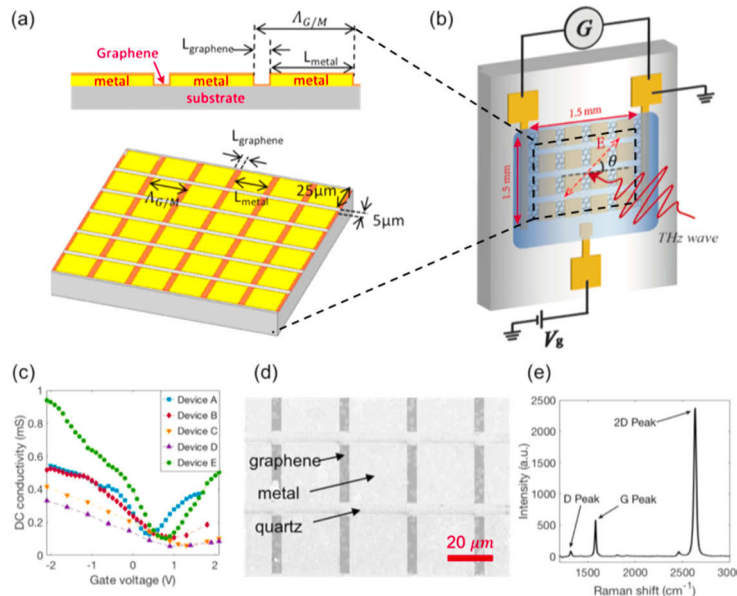


Fig. 1. (a) Schematic diagram of the graphene-metal hybrid wire grid structure. Upper figure: cross-section of the array, lower figure: top view of the array. (b) Schematic diagram of the THz transmission experiment: the lower electrode was used for applying gate voltage and the upper two electrodes were connected to a source meter for measuring the conductivity (indicated by G) (c) DC conductivities of graphene in each device as a function of gate voltage. (d) SEM image of the graphene-metal hybrid wire grids with $\Lambda_{M/G} = 30 \mu m$. (e) Raman spectrum of the graphene in a typical device.

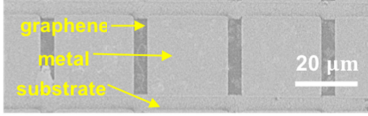
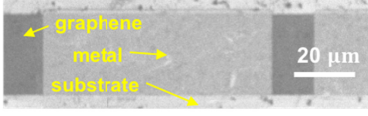
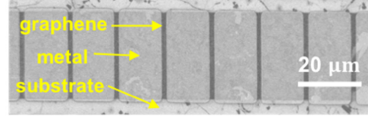
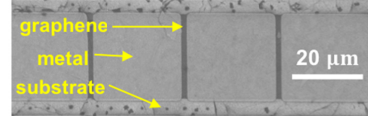
The transmission of the graphene-metal hybrid wire grid can be calculated by $t = t_d \times t_p$, where t_d and t_p are the transmission after Drude absorption and TE-polarized plasmon absorption, respectively. t_d can be calculated by $t_d(\omega) = 2n_1/(n_1 + n_2 + Z_0\sigma_s)$ [36], where σ_s is the sheet optical conductivity of the wires, and n_1 and n_2 are the refractive indices on the two sides of the wire grids, while t_p can be calculated by $t_p(\omega) = 2\sqrt{Y_1 Y_2}/|Y_1 + Y_2 + Y(\omega)|$ [35], where Y_1 and Y_2 are the inverse of the characteristic impedance of materials on both sides of the wire grids, and $Y(\omega)$ is the complex admittance of the graphene-metal LC circuit. All theoretical results in this work were calculated based on the equations above.

2.2. Fabrication and measurement methods

Five devices of different geometries, as described in Table 1, were fabricated to investigate their effect on the polarizer performance. Devices A, B, and C were fabricated to show the effect of changing $\Lambda_{G/M}$, while devices A, D, and E demonstrated the effects of changing GFF.

Figure 1(b) shows a schematic diagram of the THz transmission experiment used to investigate the polarizer response. θ is the angle between the incoming THz wave electric field polarization and the wire orientation. $\theta = 0^\circ$ represents TE polarization, while $\theta = 90^\circ$ represents TM polarization. The upper two metal contacts connecting to either end of the wires were used to measure the DC conductance of the wire grid, which was then used to calculate the conductivity, based on the wire geometry. The lower metal contact was used to apply a gate voltage, enabling conductivity modulation. The polarizers were fabricated on a 0.35 mm thick ST-cut SSP quartz substrate. The metal patterns were fabricated first using direct-write DLP laser lithography (MLA150, Heidelberg Instruments) followed by electron-beam evaporation with Ti/Au (7nm/70nm) layers. CVD graphene samples on copper were then transferred onto the

Table 1. Geometric parameters of the graphene-metal hybrid polarizers fabricated in this work.

Our device	L_{graphene} (μm)	$\Lambda_{\text{G/M}}$ (μm)	SEM images	GFF
Device A	5	30		1/6
Device B	15	90		1/6
Device C	2.5	15		1/6
Device D	2.5	27.5		1/11
Device E	Graphene Wires Only			/

metal arrays following a wet transfer procedure [37,38]; Poly- (methyl methacrylate) (PMMA) was spin coated as a support, and the copper foil was then removed using 2% ammonium persulfate solution. The graphene initially covered the whole metal metasurface area, which was $1.5\text{mm} \times 1.5\text{mm}$. The graphene was then etched into the wire-grid structures using oxygen plasma at a power of 50 W for 2 minutes, with the graphene wires protected by S1813 photoresist, which was removed in acetone after etching. Devices were electrically tuned using an ion gel (a mixture of 2 parts of 1-ethyl-3-methylimidazolium bis(trifluoromethylsulfonyl)imide ([EMIM][TFSI]) and 1 part of poly(vinylidene fluoride-co-hexafluoropropylene) (PVDF-HFP) by weight) applied as the gate dielectric material; this gel has previously shown good transparency for THz waves [24] along with the ability to induce a large carrier density at low gate voltage [39]. The ion gel was prepared by dissolving PVDF-HFP in acetone with the aid of a magnetic stirrer for an hour, before adding the [EMIM][TFSI] into the solution and stirring for 24 hrs. The prepared ion gel was then drop-cast on to the gratings, and dried in ambient conditions for one hour [40].

The gate voltage-dependent DC conductivity of the graphene in each device was measured directly using a source-measurement unit, yielding the data shown in Fig. 1(c). The devices were imaged using SEM and characterized using Raman microscopy after THz transmission measurements. Examples of the SEM image of the wire grids, and the Raman spectrum of

graphene in the polarizer, are shown in Figs. 1(d) and 1(e), respectively. The dark regions between the metal patches in the SEM image are graphene, as confirmed by the Raman spectra, in which the 2D peak was much larger than G peak, verifying the presence of single-layer graphene [41].

A THz time-domain spectroscopy (THz-TDS) system was used for transmission measurements. In this system both the THz emitter and detector were bow-tie pattern LT-GaAs photoconductive (PC) antennas, comprising a 2- μm -thick layer of LT-GaAs transferred on to a 5-mm-thick quartz substrate, fabricated using an epitaxial lift-off method [42]. The transmission characteristic of each polarizer device was obtained by dividing the Fourier transform of the transmitted THz pulse to a reference obtained from a quartz substrate with an identical layer of ion gel.

3. Results and discussion

Figure 2(a) show the normalized transmission of device A at 0.5 THz; a polarization-dependent THz transmission was found, with minimum transmission for the TE polarization and maximum transmission for the TM polarization. DC transport measurements showed that the graphene Fermi level in device A reached the Dirac point at a gate bias of 0.4 V (Fig. 1(c)). The THz transmission was obtained for different gate voltages, as shown in Fig. 2(b), with examples of the time-domain THz pulses passing through the polarizer shown as insets. As anticipated, the largest transmission changes were observed for $\theta = 0^\circ$; the transmission gradually reduced with increasing θ up to $\theta = 90^\circ$, at which the point transmission curves at different gate voltages essentially overlapped. The modulation depth (MD), shown in Fig. 2(c), was obtained by $MD = (T_D - T)/T_D$, where T_D is the transmission when $V_g = V_{Dirac}$ and T is the transmission of the polarizer, here obtained when $V_g = -2.1V$. As expected, the largest transmission modulation was seen for the TE polarization, with the modulation gradually reducing as θ was increased to 90° . The inset of Fig. 2(c) presents the polarization-dependent MD at 0.5 THz. The MD of the TE transmission reached a value of $\sim 44\%$ for device A for frequencies between 0.5–1.5 THz, while the MD of the TM transmission was found to be negligible.

Figure 2(d) shows the suppression of the MD of the TM transmission when $L_{graphene}$ is reduced. For a graphene wire grid, device E, the MD of TM transmission was around 14% to 21% (red solid line), while when $L_{graphene}$ was reduced, the MD of TM transmission was also reduced (green and blue solid line). For the 25- μm -wide wires, the MD of TM transmission was found to be negligible when $L_{graphene}$ was smaller than 5 μm . Since, as expected, the MD of TM transmission was negligible, the following discussions will focus on the MD of the TE transmission. We note that the modulation speed of an ion-gel gating device such as ours is limited by the electrical characteristics of the ion gel. The operation speed of the ion gel we used in this work was found to be ~ 300 Hz, reported by K. Chae *et al* [40]. This modulation speed is relatively slow compared to the conventional field-effect transistor based modulator [43], which can show several kHz operation, but the modulation speed of our device could be significantly increased (up to ~ 10 kHz) by replacing the polymer in the ion gel from the PVDF-HFR used with PS-PEO-PS triblock copolymer [44].

The working bandwidth of the polarizer was limited by the period of the graphene-metal grid, $\Lambda_{G/M}$, since the metal patch array acts as a low-pass filter with a cut-off frequency determined by its period [45,46]. To investigate this, three devices (devices A, B, and C) with different $\Lambda_{G/M}$ were tested as shown in Fig. 3. The MD was obtained by tuning the gate voltage $V_g = V_{Dirac}$ to $V_g = -2.1V$ in each case. The cut-off frequencies of the experimental data in Fig. 3 were found to be similar to the theoretical cut-off frequencies of the metal patch arrays as shown in Table 2, indicating that the period of the metal array was predominantly determined by the bandwidth of the polarizers. Here, the cut-off frequencies were calculated using their relationship with the period of the metal array ($f_{cut-off} = c/n_{eff} \cdot \Lambda_{G/M}$, where c is the speed of light, and n_{eff} is an effective refractive index). As such, to obtain broader bandwidth, a shorter $\Lambda_{G/M}$ would be required. Among the fabricated devices, the largest bandwidth was obtained by device C,

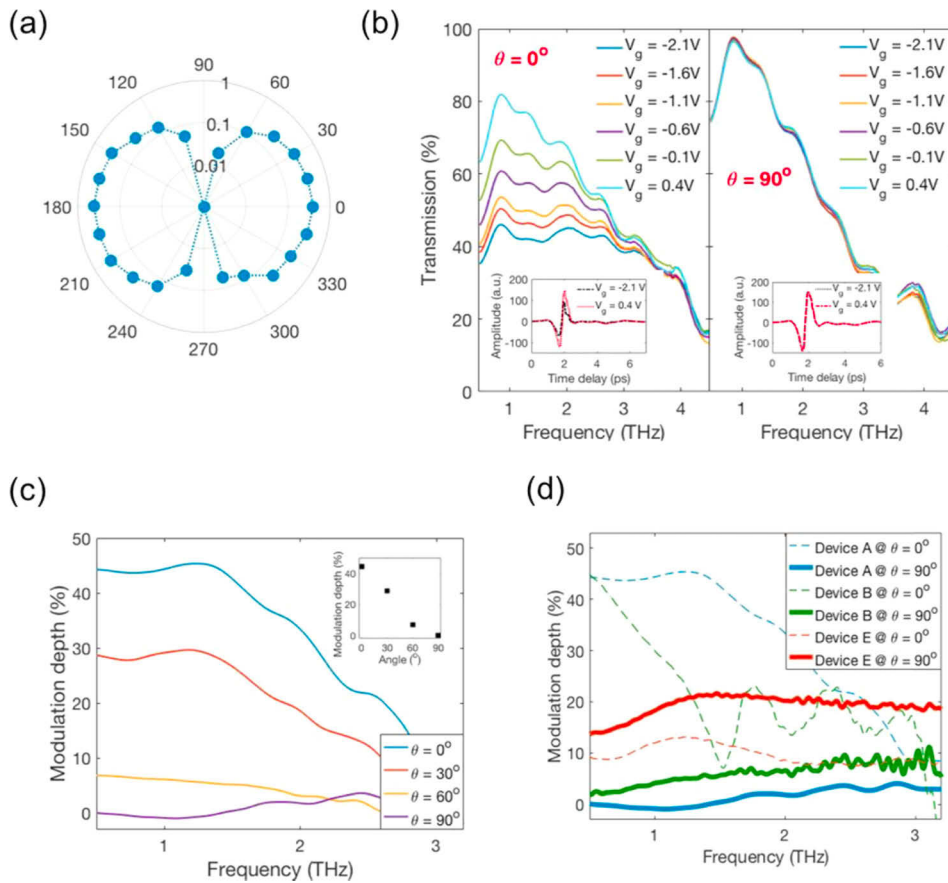


Fig. 2. (a) Normalized transmission $(T_{TM} - T_{pol})/T_{TM}$ of the THz polarizer (device A), where T_{TM} and T_{pol} are the TM transmission and the polarizer transmission, respectively. In this polar coordinate, the angle is that of the polarization with respect to the TE polarization, and the magnitude represents the normalized transmission for 0.5 THz. (b) Frequency-domain transmission obtained at different gate voltages and for polarization $\theta = 0^\circ$ and $\theta = 90^\circ$. Inset: transmitted time-domain THz pulses. (c) Modulation depth of device A as a function of frequency with polarization θ between 0° and 90° with respect to the TE polarization. Inset: modulation depth at 0.5 THz as a function of angle theta. (d) Comparison of the modulation depth observed in devices A, B and E as a function of frequency for TE polarized and TM polarized THz waves.

with $\Lambda_{G/M} = 15\mu m$. The bandwidth of this device extended across the whole bandwidth of our TDS system, ~ 5 THz. The fractional bandwidths were also estimated in Table 2 to evaluate our devices. We obtained a fractional bandwidth of ~ 1.6 with the device C, which may be categorized as ultra-wideband [47].

Table 2. Experimental cut-off frequency and fractional bandwidth of devices A, B and C, and the theoretical cut-off frequency of the metal patch arrays with the corresponding geometries.

Geometry	Experiments of polarizer	Fractional bandwidth	Calculation of metal array
Device A	4.3 THz	1.6	4.75 THz
Device B	1.53 THz	1.0	1.58 THz
Device C	> 5 THz	>1.6	9.5 THz

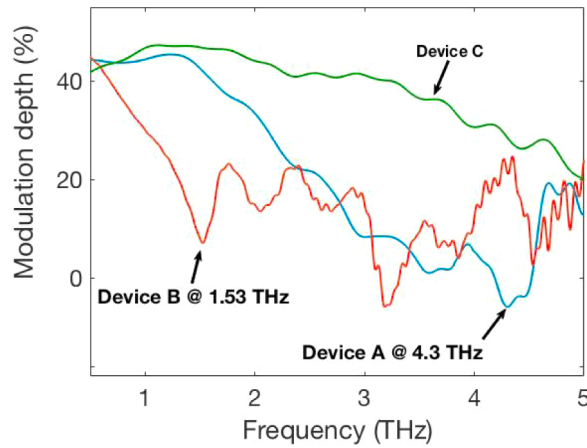


Fig. 3. Modulation depths of device A (blue), device B (red), and device C (green) obtained in the experiment.

To investigate the modulation enhancement by introducing the metal metasurface into the graphene wire grid, device A and device D with different GFF to compare with device E (graphene wire only device). The MD of these devices as the gate voltage was changed from V_{Dirac} to -2.1 V were measured and theoretically calculated as shown in Figs. 4(a) and 4(b), respectively. Compared with device E, in which no metal metasurface was introduced, device A showed an approximately four times greater MD at 0.5–1.5 THz, and device D showed an approximately ~six times greater MD at 0.5–2.5 THz. This demonstrates that a smaller GFF induces a considerably greater modulation, as expected. The PER of device D was modulated from 3.7 dB to 10.3 dB obtained from $PER = 20\log(T_{TM}/T_{TE})$, where T_{TM} and T_{TE} were the TM transmission and TE transmission amplitudes, respectively. The maximum PER was obtained when $V_g = -2.1$ V, and minimum when $V_g = V_{Dirac}$, which was 0.9 V for device D. The PER value obtained here (~10 dB) is below compared to that of metal wire grid (20 - 40 dB), though still slightly better than tunable device using graphene/insulator stacks (9.5 dB) [48]. We note that our design thus shows a significantly enhanced PER when compared to devices that integrate sheet graphene with metal patch arrays, in which only ~0.7 dB of PER has been obtained [49].

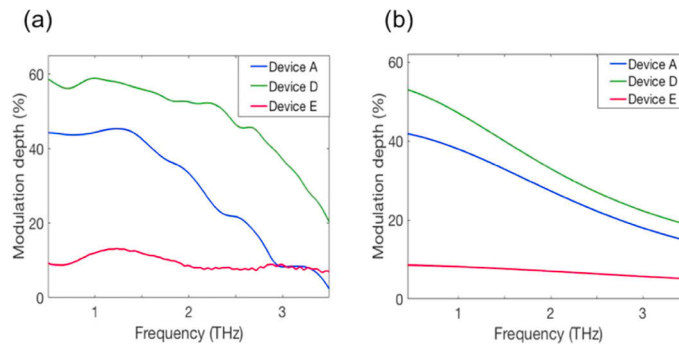


Fig. 4. Modulation depth of device A (blue), device D (green) and device E (red) with respect to frequency, obtained (a) experimentally, and (b) by calculation.

Comparing the experimental and theoretical transmission results (Fig. 4), we note several differences, notwithstanding their overall similarity. First, the measured MD is up to ~3% larger

than that calculated for low frequencies. This is likely to be a result of the contact resistance between graphene and metal, causing the dc conductivity used in the calculation to be smaller than the sheet conductivity. Second, the measured MD decays somewhat more slowly with frequency than the calculated results. This could be caused by impurities and vacancies in the graphene, which may affect the optical conductivity and plasmon excitations [50] by the introduction of additional carrier scattering. Additionally, we observe a slight oscillatory behavior in the experimental data, likely to be caused by interference of the THz pulse caused by the reflection the surfaces (substrate and ion gel). In addition, a more rapid MD decrease with respect to frequency was observed for frequencies above 3 THz in experiments owing to the limited system bandwidth, which rolled off beyond 3 THz.

The transmission modulation was found to be proportional to the graphene conductivity (Fig. 5), and we used the gradient of the curves of MD versus conductivity ($\Delta MD / \Delta \sigma_{graphene}$) to quantify the modulation ability of the polarizers. We note that the key factor here is the slope since we quantify the modulation ability using it. The maximum modulation ability enhancement came from device D, which had the smallest GFF, while the modulation ability enhancement compared to the device without any metal metasurface (device E) was found to be $17.8 \times$ according to the experiment, and $18.0 \times$ according to calculation.

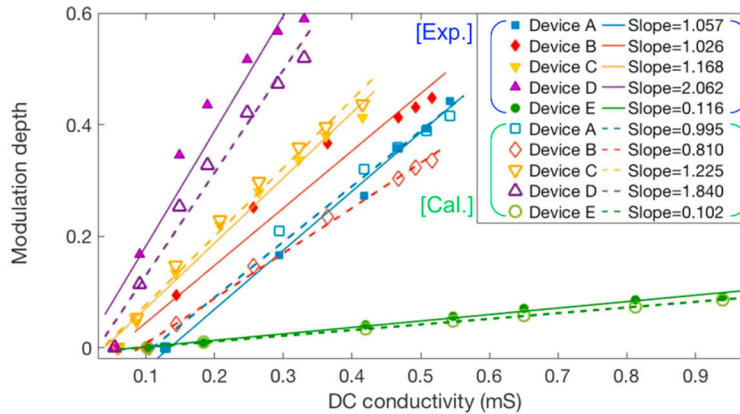


Fig. 5. Modulation depth at 0.5 THz as a function of graphene conductivity for polarizers with different periods and graphene filling factors obtained in experiments (filled symbols), and in calculations (open symbols).

The MD and the working bandwidth of the polarizer could be improved by further reducing the GFF and the $\Delta_{G/M}$, which we investigated theoretically. We considered graphene dimensions from 10 nm to 10 μm , noting that the former could potentially be realized experimentally using e-beam lithography [51]. The GFF were set from 0.001 to 0.5 while the graphene conductivity was varied between 0.1 mS and 20 mS [36]. The calculated MDs at 0.5 THz are shown in Fig. 6. Based on these parameters, the maximum MD found to be possible was 99.997%, employing 10 nm graphene with a 10 μm period.

Aside from the MD, other performance parameters such as the bandwidth and transmission of the polarizer also change when the geometries are changed. To investigate this theoretically, several different geometries were investigated, realized to obtain a range MDs as shown in Fig. 6; the results are summarized in Table 3. It can be seen that either a shorter $L_{graphene}$ or larger GFF results in a broader bandwidth (reaching as high as >90 THz for geometry 1 in Table 3), while smaller GFF results in smaller TE transmission, indicating a higher PER (eg. up to ~ 70 dB for geometry 5). Here, the modulation bandwidth here is determined by the structural factors such as GFF rather than gating method. The possible PER of our design is up to 30 dB higher than

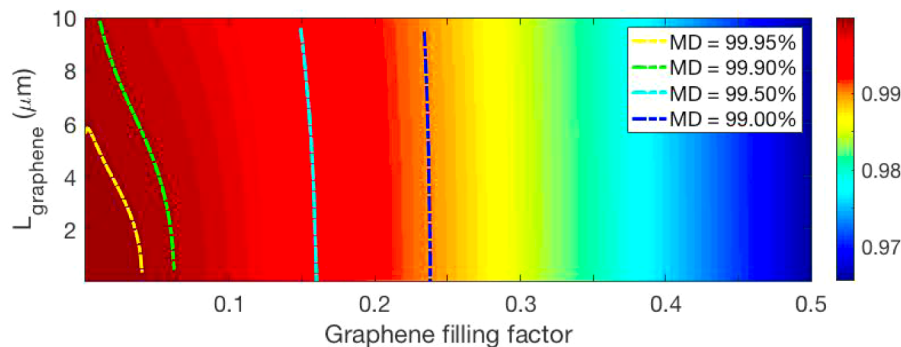


Fig. 6. Colour-scale plot showing the modulation depth MD at 0.5 THz as a function of the length of graphene (ranging from 10 nm to 10 μ m) and graphene filling factors (ranging from 0.001 to 0.5); the MD value is indicated in the color bar.

commercial metal wire grid THz polarizers (20–40 dB). By a suitable choice of geometry, the proposed polarizers can thus target either maximal bandwidth, maximal PER, or a compromise between these factors according to the needs of particular applications. We note that fabrication of the smaller devices could not be achieved using our current patterning method (direct-write DLP laser lithography) owing to its resolution limit of $\sim 1 \mu\text{m}$. We anticipate that these devices could be fabricated using alternative methods such as high-resolution deep UV lithography in the future work, or by electron beam lithography, though we note the latter would be time-consuming for our device with patterned area of $1.5\text{mm} \times 1.5\text{mm}$.

Table 3. Performance of THz polarizers producing a 99.9% modulation depth for different geometric parameters.

Geometry	L_{graphene} (μm)	GFF	$\Lambda_{\text{G/M}}$ (μm)	Max / min transmission	Cut-off frequency (THz)	Min / max PER (dB)
1	0.1	0.064	1.56	0.557 / 5.85E-4	91.3	4.5 / 62
2	0.5	0.062	8.06	0.55 / 5.50E-4	17.7	4.7 / 63
3	2.3	0.059	38.98	0.499 / 5.00E-4	3.66	5.5 / 64
4	4.0	0.052	76.92	0.389 / 3.91E-4	1.85	7.7 / 66
5	6.0	0.037	162.16	0.202 / 2.01E-4	0.88	13 / 72

4. Conclusions

A new tunable broadband THz polarizer with a geometry comprising a graphene-metal hybrid metasurface was designed, fabricated, and characterized. We experimentally verified its broadband, polarization-dependent, and electrically tunable THz transmission modulation. We demonstrated a significant enhancement of THz transmission modulation in this device, which gave a ~ 17 times modulation ability enhancement in the frequency ranging from 0.5 THz to 2.5 THz compared to graphene wire arrays. Theory indicates that the performance of the polarizer could be further improved by reducing the dimensions, allowing the structures to satisfy applications where either ultra-broadband modulation or ultra-high PER are required. Our device could be applied as a polarization sensitive THz switch or attenuator in THz communication circuits, for example, and could also be extended to a wider range of operating frequency by controlling the geometrical parameters in the ways suggested, while noting that no current efficient THz source or detector combination is yet available which would extend across the entire potential working frequency range of this form of polarizer (from 0.1 to >90 THz).

Funding

Engineering and Physical Sciences Research Council (EP/P007449/1, EP/P021859/1, EP/R00501X/1).

Acknowledgments

EHL acknowledges support from the Royal Society and Wolfson Foundation. The authors would like to thank Timothy Moorsom and Oscar Cepedes for their help with Raman microscopy. Data set is online at <https://doi.org/10.5518/704>.

Disclosures

The authors declare no conflicts of interest.

References

1. F. Zangeneh-Nejad and R. Safian, "Significant enhancement in the efficiency of photoconductive antennas using a hybrid graphene molybdenum disulphide structure," *J. Nanophotonics* **10**(3), 036005 (2016).
2. S. H. Lee, M. Choi, T. T. Kim, S. Lee, M. Liu, X. Yin, H. K. Choi, S. S. Lee, C. G. Choi, S. Y. Choi, X. Zhang, and B. Min, "Switching terahertz waves with gate-controlled active graphene metamaterials," *Nat. Mater.* **11**(11), 936–941 (2012).
3. H. Tao, N. I. Landy, C. M. Bingham, X. Zhang, R. D. Averitt, and W. J. Padilla, "A metamaterial absorber for the terahertz regime: Design, fabrication and characterization," *Opt. Express* **16**(10), 7181–7188 (2008).
4. K. Meng, S. J. Park, A. D. Burnett, T. Gill, C. D. Wood, M. Rosamond, L. H. Li, L. Chen, D. R. Bacon, J. R. Freeman, P. Dean, Y. H. Ahn, E. H. Linfield, A. G. Davies, and J. E. Cunningham, "Increasing the sensitivity of terahertz split ring resonator metamaterials for dielectric sensing by localized substrate etching," *Opt. Express* **27**(16), 23164–23172 (2019).
5. S. J. Park, J. T. Hong, S. J. Choi, H. S. Kim, W. K. Park, S. T. Han, J. Y. Park, S. Lee, D. S. Kim, and Y. H. Ahn, "Detection of microorganisms using terahertz metamaterials," *Sci. Rep.* **4**(1), 4988 (2015).
6. F. Zangeneh-Nejad and R. Safian, "A Graphene-Based THz Ring Resonator for Label-Free Sensing," *IEEE Sens. J.* **16**(11), 4338–4344 (2016).
7. N. C. J. van der Valk, W. A. M. van der Marel, and P. C. M. Planken, "Terahertz polarization imaging," *Opt. Lett.* **30**(20), 2802–2804 (2005).
8. T. T. Kim, S. S. Oh, H. D. Kim, H. S. Park, O. Hess, B. Min, and S. Zhang, "Electrical access to critical coupling of circularly polarized waves in graphene chiral metamaterials," *Sci. Adv.* **3**(9), 1701377 (2017).
9. C. F. Hsieh, Y. C. Lai, R. P. Pan, and C. L. Pan, "Polarizing terahertz waves with nematic liquid crystals," *Opt. Lett.* **33**(11), 1174–1176 (2008).
10. A. Wojdyla and G. Gallot, "Brewster's angle silicon wafer terahertz linear polarizer," *Opt. Express* **19**(15), 14099–14107 (2011).
11. A. Ferraro, D. C. Zografopoulos, M. Missori, M. Peccianti, R. Caputo, and R. Beccherelli, "Flexible terahertz wire grid polarizer with high extinction ratio and low loss," *Opt. Lett.* **41**(9), 2009–2012 (2016).
12. A. Zubair, D. E. Tsentalovich, C. C. Young, M. S. Heimbeck, H. O. Everitt, M. Pasquali, and J. Kono, "Carbon nanotube fiber terahertz polarizer," *Appl. Phys. Lett.* **108**(14), 141107 (2016).
13. T. J. Guo and C. Argyropoulos, "Broadband polarizers based on graphene metasurfaces," *Opt. Lett.* **41**(23), 5592–5595 (2016).
14. Z. Q. Li, E. A. Henriksen, Z. Jiang, Z. Hao, M. C. Martin, P. Kim, H. L. Stormer, and D. N. Basov, "Dirac charge dynamics in graphene by infrared spectroscopy," *Nat. Phys.* **4**(7), 532–535 (2008).
15. C. J. Docherty and M. B. Johnston, "Terahertz Properties of Graphene," *J. Infrared, Millimeter, Terahertz Waves* **33**(8), 797–815 (2012).
16. P. Tassin, T. Koschny, and C. M. Soukoulis, "Graphene for Terahertz Applications," *Science* **341**(6146), 620–621 (2013).
17. L. Ju, B. S. Geng, J. Horng, C. Girit, M. Martin, Z. Hao, H. A. Bechtel, X. G. Liang, A. Zettl, Y. R. Shen, and F. Wang, "Graphene plasmonics for tunable terahertz metamaterials," *Nat. Nanotechnol.* **6**(10), 630–634 (2011).
18. X. Y. He, F. Liu, F. T. Lin, and W. Z. Shi, "Graphene patterns supported terahertz tunable plasmon induced transparency," *Opt. Express* **26**(8), 9931–9944 (2018).
19. T. Low and P. Avouris, "Graphene Plasmonics for Terahertz to Mid-Infrared Applications," *ACS Nano* **8**(2), 1086–1101 (2014).
20. Y. V. Bludov, M. I. Vasilevskiy, and N. M. R. Peres, "Tunable graphene-based polarizer," *J. Appl. Phys.* **112**(8), 084320 (2012).
21. H. T. Chen, A. J. Taylor, and N. F. Yu, "A review of metasurfaces: physics and applications," *Rep. Prog. Phys.* **79**(7), 076401 (2016).
22. Y. Zhang, Y. J. Feng, B. Zhu, J. M. Zhao, and T. Jiang, "Switchable quarter-wave plate with graphene based metamaterial for broadband terahertz wave manipulation," *Opt. Express* **23**(21), 27230–27239 (2015).

23. L. Deng, Y. G. Wu, C. Zhang, W. J. Hong, B. Peng, J. F. Zhu, and S. F. Li, "Manipulating of Different-Polarized Reflected Waves with Graphene-based Plasmonic Metasurfaces in Terahertz Regime," *Sci. Rep.* **7**(1), 10558 (2017).
24. Z. Q. Miao, Q. Wu, X. Li, Q. He, K. Ding, Z. H. An, Y. B. Zhang, and L. Zhou, "Widely Tunable Terahertz Phase Modulation with Gate-Controlled Graphene Metasurfaces," *Phys. Rev. X* **5**(4), 041027 (2015).
25. T. B. Sun, J. W. Kim, J. M. Yuk, A. Zettl, F. Wang, and C. Chang-Hasnain, "Surface-normal electro-optic spatial light modulator using graphene integrated on a high-contrast grating resonator," *Opt. Express* **24**(23), 26035–26043 (2016).
26. T. Nagatsuma, G. Ducournau, and C. C. Renaud, "Advances in terahertz communications accelerated by photonics," *Nat. Photonics* **10**(6), 371–379 (2016).
27. L. J. Cheng and L. Liu, "Optical modulation of continuous terahertz waves towards cost-effective reconfigurable quasi-optical terahertz components," *Opt. Express* **21**(23), 28657–28667 (2013).
28. F. Yan, C. Yu, H. Park, E. P. J. Parrott, and E. Pickwell-MacPherson, "Advances in Polarizer Technology for Terahertz Frequency Applications," *J. Infrared, Millimeter, Terahertz Waves* **34**(9), 489–499 (2013).
29. K. Imakita, T. Kamada, M. Fujii, K. Aoki, M. Mizuhata, and S. Hayashi, "Terahertz wire grid polarizer fabricated by imprinting porous silicon," *Opt. Lett.* **38**(23), 5067–5070 (2013).
30. J. H. Hu, Y. Q. Huang, X. F. Duan, Q. Wang, X. Zhang, J. Wang, and X. M. Ren, "Enhanced absorption of graphene strips with a multilayer subwavelength grating structure," *Appl. Phys. Lett.* **105**(22), 221113 (2014).
31. J. Wu, "Enhancement of Absorption in Graphene Strips With Cascaded Grating Structures," *IEEE Photonics Technol. Lett.* **28**(12), 1332–1335 (2016).
32. M. Grande, G. V. Bianco, M. A. Vincenti, D. de Ceglia, P. Capezzuto, M. Scalora, A. D'Orazio, and G. Bruno, "Optically Transparent Microwave Polarizer Based On Quasi-Metallic Graphene," *Sci. Rep.* **5**(1), 17083 (2015).
33. J. W. You and N. C. Panoiu, "Polarization control using passive and active crossed graphene gratings," *Opt. Express* **26**(2), 1882–1894 (2018).
34. Y. Y. Xia, Y. Y. Dai, B. Wang, A. Chen, Y. B. Zhang, Y. W. Zhang, F. Guan, X. H. Liu, L. Shi, and J. Zi, "Polarization dependent plasmonic modes in elliptical graphene disk arrays," *Opt. Express* **27**(2), 1080–1089 (2019).
35. M. M. Jadidi, A. B. Sushkov, R. L. Myers-Ward, A. K. Boyd, K. M. Daniels, D. K. Gaskill, M. S. Fuhrer, H. D. Drew, and T. E. Murphy, "Tunable Terahertz Hybrid Metal-Graphene Plasmons," *Nano Lett.* **15**(10), 7099–7104 (2015).
36. B. Sensale-Rodriguez, T. Fang, R. S. Yan, M. M. Kelly, D. Jena, L. Liu, and H. L. Xing, "Unique prospects for graphene-based terahertz modulators," *Appl. Phys. Lett.* **99**(11), 113104 (2011).
37. G. B. Barin, Y. Song, I. D. Gimenez, A. G. Souza, L. S. Barretto, and J. Kong, "Optimized graphene transfer: Influence of polymethylmethacrylate (PMMA) layer concentration and baking time on graphene final performance," *Carbon* **84**, 82–90 (2015).
38. M. P. Lavin-Lopez, J. L. Valverde, A. Garrido, L. Sanchez-Silva, P. Martinez, and A. Romero-Izquierdo, "Novel etchings to transfer CVD-grown graphene from copper to arbitrary substrates," *Chem. Phys. Lett.* **614**, 89–94 (2014).
39. B. J. Kim, H. Jang, S. K. Lee, B. H. Hong, J. H. Ahn, and J. H. Cho, "High-Performance Flexible Graphene Field Effect Transistors with Ion Gel Dielectrics," *Nano Lett.* **10**(9), 3464–3466 (2010).
40. K. Chae, N. D. Cuong, S. Ryu, D. I. Yeom, Y. H. Ahn, S. Lee, and J. Y. Park, "Electrical properties of ion gels based on PVDF-HFP applicable as gate stacks for flexible devices," *Curr. Appl. Phys.* **18**(5), 500–504 (2018).
41. A. C. Ferrari, J. C. Meyer, V. Scardaci, C. Casiraghi, M. Lazzeri, F. Mauri, S. Piscanec, D. Jiang, K. S. Novoselov, S. Roth, and A. K. Geim, "Raman spectrum of graphene and graphene layers," *Phys. Rev. Lett.* **97**(18), 187401 (2006).
42. D. R. Bacon, A. D. Burnett, M. Swithenbank, C. Russell, L. Li, C. D. Wood, J. Cunningham, E. H. Linfield, A. G. Davies, P. Dean, and J. R. Freeman, "Free-space terahertz radiation from a LT-GaAs-on-quartz large-area photoconductive emitter," *Opt. Express* **24**(23), 26986–26997 (2016).
43. Q. Mao, Q. Y. Wen, W. Tian, T. L. Wen, Z. Chen, Q. H. Yang, and H. W. Zhang, "High-speed and broadband terahertz wave modulators based on large-area graphene field-effect transistors," *Opt. Lett.* **39**(19), 5649–5652 (2014).
44. J. H. Cho, J. Lee, Y. Xia, B. Kim, Y. He, M. J. Renn, T. P. Lodge, and C. Daniel Frisbie, "Printable ion-gel gate dielectrics for low-voltage polymer thin-film transistors on plastic," *Nat. Mater.* **7**(11), 900–906 (2008).
45. J. E. Heyes, W. Withayachumnankul, N. K. Grady, D. R. Chowdhury, A. K. Azad, and H. T. Chen, "Hybrid metasurface for ultra-broadband terahertz modulation," *Appl. Phys. Lett.* **105**(18), 181108 (2014).
46. O. Luukkonen, C. Simovski, G. Granet, G. Goussetis, D. Lioubtchenko, A. V. Raisanen, and S. A. Tretyakov, "Simple and accurate analytical model of planar grids and high-impedance surfaces, comprising metal strips or patches," *IEEE Trans. Antennas Propag.* **56**(6), 1624–1632 (2008).
47. H. Arslan, Z. N. Chen, and M. G. Di Benedetto, *Ultra Wideband Wireless Communication* (John Wiley and Sons, 2005).
48. H. Yan, X. Li, B. Chandra, G. Tulevski, Y. Wu, M. Freitag, W. Zhu, P. Avouris, and F. Xia, "Tunable infrared plasmonic devices using graphene/insulator stacks," *Nat. Nanotechnol.* **7**(5), 330–334 (2012).
49. I. T. Lin, J. M. Liu, H. C. Tsai, K. H. Wu, J. Y. Syu, and C. Y. Su, "Family of graphene-assisted resonant surface optical excitations for terahertz devices," *Sci. Rep.* **6**(1), 35467 (2016).
50. G. Viola, T. Wenger, J. Kinaret, and M. Fogelstrom, "Graphene plasmons: Impurities and nonlocal effects," *Phys. Rev. B* **97**(8), 085429 (2018).
51. C. Vieu, F. Carcenac, A. Pepin, Y. Chen, M. Mejias, A. Lebib, L. Manin-Ferlazzo, L. Couraud, and H. Launois, "Electron beam lithography: resolution limits and applications," *Appl. Surf. Sci.* **164**(1-4), 111–117 (2000).